# Loss function of tumor suppressor FRMD8 confers resistance to tamoxifen therapy via a dual mechanism

Weijie Wu[1#], Miao Yu[1#], Qianchen Li[1], Yiqian Zhao[1], Lei Zhang[1], Yi Sun[1], Zhenbin Wang[1], Yuqing Gong[1], Wenjing Wang[2], Chenying Liu[3], Jing Zhang[1], Yan Tang[1], Xiaojie Xu[4]*, Xiaojing Guo[3]*; Jun Zhan[1]*, Hongquan Zhang[1]*

[1]Program for Cancer and Cell Biology, Department of Human Anatomy, Histology and Embryology, School of Basic Medical Sciences; Peking University International Cancer Institute; and State Key Laboratory of Molecular Oncology, Peking University Health Science Center, Beijing 100191, China.

[2]Department of Gastroenterology, Beijing Friendship Hospital, Capital Medical University; State Key Laboratory for Digestive Health; National Clinical Research Center for Digestive Diseases，Beijing 100050, China.

[3]Department of Breast Pathology and Lab; Tianjin Medical University Cancer Institute & Hospital; National Clinical Research Center for Cancer; Key Laboratory of Breast Cancer Prevention and Therapy of Ministry of Education of China, Tianjin Medical University; Tianjin's Clinical Research Center for Cancer, Tianjin 300060, China.

[4]Department of Genetic Engineering, Beijing Institute of Biotechnology, Beijing 100071, China.

# These two authors contributed equally to this study.

Running title: Loss of FRMD8 downregulates ERα level

Word number of texts: 7,239

Characters with space: 49,894

* Corresponding authors

Hongquan Zhang, Ph.D.; Professor
Peking University Health Science Center,
#38 Xue Yuan Road, Haidian District, Beijing 100191, China.
Tel: 008610-82802424, E-mail: Hongquan.Zhang@bjmu.edu.cn
Or
Jun Zhan, M.D. & Ph.D.; Associate Professor
Peking University Health Science Center,
#38 Xue Yuan Road, Haidian District, Beijing 100191, China.
E-mail: Zhanjun@bjmu.edu.cn

36 Or
37 Xiaojing Guo, M.D. & Ph.D.
38 Tianjin Medical University Cancer Institute & Hospital,
39 West Huanhu Road, Tianjin 300060, China.
40 E-mail: guoxiaojing@tjmuch.com
41 Or
42 Xiaojie Xu, M.D. & Ph.D.; Associate Professor
43 Department of Genetic Engineering, Beijing Institute of Biotechnology,
44 Beijing 100071, China.
45 E-mail: miraclexxj@126.com
46
47

## Abstract

Approximately 40% ERα-positive breast cancer patients suffer from therapeutic resistance to tamoxifen. Although reduced ERα level is the major cause of tamoxifen resistance, the underlying mechanisms remain elusive. Here, we report that FRMD8 raises the level of ERα at both transcriptional and post-translational layers. FRMD8 deficiency in *MMTV-Cre*$^{+}$; *Frmd8*$^{fl/fl}$; *PyMT* mice accelerates mammary tumor growth and loss of luminal phenotype, and confers tamoxifen resistance. Single-cell RNA profiling reveals that Frmd8 loss decreases the proportion of hormone-sensing differentiated epithelial cells and downregulates the levels of ERα. Mechanically, on one hand, loss of FRMD8 inhibits *ESR1* transcription via suppressing the expression of FOXO3A, a transcription factor of *ESR1*. On the other hand, FRMD8 interacts both with ERα and UBE3A, and disrupts the interaction of UBE3A with ERα, thereby blocking UBE3A-mediated ERα degradation. In breast cancer patients, *FRMD8* gene promoter is found hypermethylated and low level of FRMD8 predicts poor prognosis. Therefore, FRMD8 is an important regulator of ERα and may control therapeutic sensitivity to tamoxifen in ERα-positive breast cancer patients.

Keywords: FRMD8; Breast cancer; ERα; Tamoxifen resistance; UBE3A

## Introduction

Breast cancer is the most commonly diagnosed cancer worldwide(Sung in drugi, 2021) and more than 70% of breast cancer are estrogen receptor α (ERα)-positive(Habara in Shimada, 2022). Although endocrine therapy is the most common systemic treatment for ERα-positive breast cancer in clinical practice, approximately 40% of patients still develop primary or secondary resistance to endocrine therapy(Badia in drugi, 2007; Légaré in Basik, 2016; Rondón-Lagos in drugi, 2016). Therefore, it is urgent and necessary to explore the mechanisms of endocrine therapy resistance and search for new therapeutic targets.

Tamoxifen (TAM), a selective estrogen receptor antagonist, is the most widely used medicine in endocrine therapy. Tamoxifen competes with estrogen to bind with ERα and changes the conformation of ERα, thereby preventing the interaction between co-activators and ERα and inhibiting activation of ERα(Katzenellenbogen in drugi, 2018). Thus, the level of ERα is strongly correlated with reactivity and resistance of endocrine therapy. Uncovering the mechanisms by which ERα expression is regulated is essential for overcoming endocrine therapy resistance. Multiple transcription factors, such as AP-2γ, FOXO3, FOXM1, and GATA3, have been reported to bind to the promoter region of *ESR1* and participate in transcriptional regulation of *ESR1*(Jia in drugi, 2019; Koš in drugi, 2001). In addition, post-translational modifications of ERα, including phosphorylation, acetylation, and ubiquitination, also have effects on subcellular localization, transcriptional activity, and stability of ERα(Rogatsky in drugi, 1999; Williams in drugi, 2009; Zhou in Slingerland, 2014). However, the mechanisms underlying the regulation of ERα expression are still not clear and require further investigation.

FERM domain-containing proteins are widely involved in processes such as the formation of macromolecular complexes, subcellular localization, functional activation, and signal transduction, thereby regulating the occurrence and development of tumors(Frame in drugi, 2010; Moleirinho in drugi, 2013; Zhan in Zhang, 2018).

FRMD8, as a member of FERM domain-containing proteins, has been reported to bind with iRhom and enhance the stability of the iRhom/TACE complex on the cell surface, thereby preventing iRhom/TACE degradation mediated by lysosomes. TACE is responsible for cleaving and releasing TNF, and the absence of FRMD8 impairs the production of TNF(Künzel in drugi, 2018; Oikonomidi in drugi, 2018). Additionally, FRMD8 expressions in both microenvironment and tumor cells promote lung tumor growth(Badenes in drugi, 2023). FRMD8 inhibits colon cancer growth by preventing cell cycle progression. FRMD8 disrupts the interaction of CDK7 with CDK4, subsequently inhibiting CDK4 activation. Furthermore, FRMD8 competes with MDM2 to bind RB, thereby attenuating MDM2-mediated RB degradation(Yu in drugi, 2023). However, the roles of FRMD8 in breast tumorigenesis and progression need further exploration.

In this study, we found that loss of Frmd8 in luminal epithelial cells of *MMTV-PyMT* mice accelerates mammary tumor progression and luminal epithelial phenotype loss, and confers tamoxifen resistance. Single-cell RNA profiling reveals that the number of hormone-sensing differentiated cells is diminished and the level of ERα is decreased in Frmd8-knocked-out mammary tumors. FRMD8 not only increases *ESR1* expression, but also prevents ERα degradation by interrupting the interaction between ERα and E3 ligase UBE3A. Further, a low FRMD8 level predicts poor prognosis in human breast cancer patients. Thus, we demonstrated that FRMD8 is an important ERα regulator and a vital tumor suppressive protein in breast cancer growth and drug resistance.

118 ## Results

119 **Loss of Frmd8 promotes mammary tumor growth and generates tamoxifen**
120 **resistance *in vivo***

121 To examine whether FRMD8 plays a role in breast tumorigenesis, we established
122 luminal epithelium-specific *Frmd8* knockout mice (*MMTV-Cre*$^{+}$; *Frmd8*$^{fl/fl}$) (Fig. 1A
123 and 1B) and further generated a Frmd8-deletion breast cancer mouse model (*MMTV-*
124 *Cre*$^{+}$; *Frmd8*$^{fl/fl}$; *PyMT*) by crossing *MMTV-Cre*$^{+}$; *Frmd8*$^{fl/fl}$ mice with *MMTV-PyMT*
125 (*PyMT*) mice, a widely used transgenic mouse model of mammary tumorigenesis (Fig.
126 1C, 1D, S1A and S1B). Compared with *MMTV-Cre*$^{-}$; *Frmd8*$^{fl/fl}$; *PyMT* mice, Frmd8
127 depleted in mice significantly promotes mammary tumor development (Fig. 1E and 1F).
128 The total tumor weight (Fig. 1G) and number of tumors (Fig. 1H) were markedly higher
129 in *MMTV-Cre*$^{+}$; *Frmd8*$^{fl/fl}$; *PyMT* mice than the control mice. Histological examination
130 of the breast tumors from *PyMT* mice using haematoxylin-eosin (H&E) staining
131 revealed that the luminal epithelium was poorly differentiated in *MMTV-Cre*$^{+}$; *Frmd8*$^{fl/fl}$;
132 *PyMT* mice tumors compared with the control mice (Fig. 1I). Furthermore,
133 immunohistochemical staining showed that the percentage of Ki67-positive cells was
134 significantly elevated in mammary tumors of *Frmd8*-depleted mice (Fig. 1J and 1K).
135 Consistently, 5-ethynyl-2'-deoxyuridine (EdU) incorporation assays demonstrated that
136 FRMD8 depletion promoted human breast cancer cell MCF7 and T47D proliferation
137 (Fig. S1C and S1D). These findings indicated that *Frmd8* deficiency in the luminal
138 epithelium accelerates mammary tumor growth in *MMTV-PyMT* mice and promotes
139 cell proliferation.

140 Since tamoxifen is commonly used for the treatment of ERα$^{+}$/HER2$^{-}$ breast cancer，
141 we thus investigated whether loss of Frmd8 affects sensitivity of mammary tumors to
142 tamoxifen treatment in mice. To this end, *MMTV-Cre*$^{-}$; *Frmd8*$^{fl/fl}$; *PyMT* mice and
143 *MMTV-Cre*$^{+}$; *Frmd8*$^{fl/fl}$; *PyMT* mice were injected intraperitoneally with tamoxifen or
144 corn oil as control every two days. The results showed that tamoxifen significantly
145 prevents mammary tumor progression in the control mice (Fig. 1L and 1M). However,

146 mammary tumors of *MMTV-Cre*$^{+}$; *Frmd8*$^{fl/fl}$; *PyMT* mice showed no response to
147 tamoxifen treatment (Fig. 1L and 1M). Consistently, the total tumor weight (Fig. 1N)
148 and number of tumors (Fig. 1O) of *MMTV-Cre*$^{-}$; *Frmd8*$^{fl/fl}$; *PyMT* mice were markedly
149 decreased after tamoxifen treatment, whereas there was no difference in *MMTV-Cre*$^{+}$;
150 *Frmd8*$^{fl/fl}$; *PyMT* mice (Fig. 1N and 1O). Taken together, these findings demonstrated
151 that loss of Frmd8 accelerates mammary tumor growth and generates resistance to
152 tamoxifen therapy in Frmd8-depleted mice.
153
154 **Frmd8 knockout decreases the proportion of the hormone-sensing differentiated**
155 **epithelial cells**
156 To investigate the mechanism through which Frmd8 loss promotes mammary tumor
157 growth and leads to tamoxifen resistance, we then performed single-cell RNA
158 sequencing (scRNA-seq) analysis. Mammary tumors from 4-month-old *MMTV-Cre*$^{-}$;
159 *Frmd8*$^{fl/fl}$; *PyMT* and *MMTV-Cre*$^{+}$; *Frmd8*$^{fl/fl}$; *PyMT* mice were harvested and analyzed
160 using the Chromium Single Cell 3' Reagent Kitsv3 (10× Genomics). Cells that passed
161 quality control (QC) filter totaled 24,320, of which 11,606 cells were from *MMTV-Cre*$^{-}$;
162 *Frmd8*$^{fl/fl}$; *PyMT*, and 12,714 cells were from *MMTV -Cre*$^{+}$; *Frmd8*$^{fl/fl}$; *PyMT* mice (Fig.
163 2A). After that, we profiled the three major cell lineages, including epithelial cells,
164 immune cells and stromal cells by the UMAP visualization (Fig. 2B). Their associated
165 top-expressed and canonical markers were shown in Figure S2A and S2B, respectively.
166 Based on the expression of known markers, a total of 12 clearly separated cell lineages
167 were finally identified (Fig. 2C and 2D). In particular, they were as follows: B cells
168 highly expressing *Cd19*, *Cd79a*, *Cd79b*; CD4$^{+}$ T cells characterized with high *Cd3g*
169 and *Cd4* expression; CD8$^{+}$ T cells highly expressing *Cd3g* and *Cd8a*; dendritic cells
170 (DCs) expressing *Cd74* and *Cd14*； endothelial cells specifically expressing the markers
171 *Pecam1* and *Emcn*; epithelial cells expressing *Epcam* and *Krt8*; fibroblast cells high
172 expressing *Col1a1* and *Col3a1*; granulocyte cells specifically expressing the markers
173 *S100a9*; macrophage cells highly expressing *Cd14*, *Cd68* and *C1qa*; monocyte cells

174 highly expressing *Cd14* and *Ccr2*; natural killer (NK) cells specifically expressing
175 *Nkg7* and *Ncr1* (Fig. S2C). The dot plots compared the proportion of cells expressing
176 cluster-specific markers and their scaled relative expression levels (Fig. S2D).

177 To further explore whether the proportions of epithelial cells in mammary tumors
178 were affected by Frmd8 loss, we subset and re-identified four epithelial cell
179 clusters(Valdes-Mora in drugi, 2021), including alveolar progenitor (Avp), basal (Bsl),
180 hormone-sensing differentiated (Hsd) and luminal progenitor (Lp) epithelial cells (Fig.
181 2E). As expected, the epithelial cells were composed of luminal epithelial cells and
182 basal epithelial cells, which were consistent with the cellular characteristics of the
183 mammary glands. In contrast to control mice, the proportion of the Hsd epithelial cells
184 was significantly decreased in *MMTV-Cre*$^{+}$; *Frmd8*$^{fl/fl}$; *PyMT* mice (Fig. 2F).

185 To define the tumor cells in the mouse mammary tumors, we applied inferCNV
186 algorithm to calculate the copy number variations (CNVs) of the single cells (Fig. 2G).
187 To this end, we analyzed CNV scores of epithelial subclusters, immune and stromal
188 cells, revealing immune cells with low CNV score (Fig. 2H). Given that Hsd epithelial
189 cells which specifically expressed *Esr1* and *Pgr* had lower CNV score than alveolar
190 progenitor (Avp), basal (Bsl) and luminal progenitor (Lp) epithelial cells, we defined
191 the low CNV score Hsd epithelial cells as normal cells (Fig. 2H and 2I). Furthermore,
192 we defined the high CNV score epithelial cells as tumor cells, and plotted the UMAP
193 visualization (Fig. 2J). The results also showed that the expression of *Frmd8* was
194 decreased in tumor cells compared with normal cells (Fig. 2K and S2E). In addition,
195 we observed that loss of Frmd8 significantly decreased the expression of *Esr1* and *Pgr*
196 in normal cells of mammary tumors, and decreased expression of Frmd8 in tumor cells
197 accompanied with low expression of *Esr1* and *Pgr* compared with normal cells (Fig.
198 2L and S2E). Taken together, these findings indicated that Frmd8 depletion in *PyMT*
199 mice leads to decreases of the Hsd epithelial cells proportion and the expression of *Esr1*
200 and *Pgr*.

201

202 **FRMD8 promotion of *ESR1* expression is mediated by FOXO3A**

203 Given that scRNA-seq results suggested that loss of Frmd8 reduced the proportion of
204 Hsd epithelial cells and the expression of *Esr1* and *Pgr*, multiple immunofluorescence
205 staining analyses were then performed to examine the change of ERα and PR at the
206 protein levels *in situ* in mammary tumors of 4-month-old Frmd8-depleted mice.
207 Consistent with the scRNA-seq results, deficiency of Frmd8 dramatically decreased the
208 levels of ERα, PR and CK8, a marker of mammary luminal epithelium, in normal
209 tissues adjacent to tumors (Fig. 3A and 3B). *In situ* tissue flow cytometry analysis
210 demonstrated that in normal tissues adjacent to tumor of the control mice, the
211 proportion of ERα-positive cells among $CK8^{+}$ cells were 45.49%, whereas this
212 proportion was just 9.28% in *MMTV-Cre*$^{+}$; *Frmd8*$^{fl/fl}$; *PyMT* mice (Fig. S3A). Similarly,
213 the proportion of PR-positive cells among $CK8^{+}$ cells was also reduced in normal
214 tissues adjacent to tumor of *MMTV-Cre*$^{+}$; *Frmd8*$^{fl/fl}$; *PyMT* mice compared with the
215 control mice (Fig. S3B). $FRMD8^{high}ER\alpha^{high}$ and $FRMD8^{high}PR^{high}$ cells were mainly
216 present in normal tissues adjacent to tumor of *MMTV-Cre*$^{-}$; *Frmd8*$^{fl/fl}$; *PyMT* mice,
217 whereas Frmd8 depletion led to $FRMD8^{low}ER\alpha^{low}$ and $FRMD8^{low}PR^{low}$ cells markedly
218 increased (Fig. S3C and S3D). In mammary tumor tissues from both control mice and
219 *MMTV-Cre*$^{+}$; *Frmd8*$^{fl/fl}$; *PyMT* mice, the expressions of ERα and PR were almost
220 negative (Fig. 3A and 3B). Since the expression of ERα is loss with tumor progression,
221 to further clarify the regulation of Frmd8 on ERα, we performed immunohistochemistry
222 (IHC) staining of mammary glands of 7-week-old *PyMT* mice, which had no palpable
223 tumors. The results showed that Frmd8 depletion also markedly decreased the
224 expression of ERα in normal and atypical hyperplasia breast tissues (Fig. S3E). Taken
225 together, these data suggested that deficiency of FRMD8 downregulates the protein
226 levels of ERα and PR in mammary tissues of *MMTV-PyMT* mice, and accelerates the
227 loss of luminal phenotype in mammary gland.

228 It was known that the common endocrine treatment for non-metastatic breast cancer
229 relies on the expression of ERα(Waks in Winer, 2019) and our results demonstrated that

230 loss of Frmd8 promotes mammary tumor growth and confers tamoxifen resistance in
231 mice, we thus aim to further examine whether FRMD8 regulates ERα expression. To
232 this end, we transiently transfect Flag-FRMD8 vector or FRMD8 siRNA in human
233 breast cancer cells. Our results showed that FRMD8 overexpression drastically
234 increased the levels of ERα, while ERα expression was greatly downregulated when
235 FRMD8 was knocked down (Fig. 3C and 3D). Moreover, qRT-PCR results indicated
236 that depletion of FRMD8 significantly decreased the mRNA level of *ESR1* (Fig. 3E).
237 FOXO3A is a crucial transcription factor for ERα(Jia in drugi, 2019). To answer
238 whether FOXO3A is involved in the regulation of FRMD8 on ERα, we examined the
239 expression of FOXO3A after silencing FRMD8 through transfecting siRNA into MCF7
240 and T47D cells. The results showed that FRMD8 silencing dramatically decreased the
241 level of FOXO3A (Fig. 3F). Consistently, overexpression of FRMD8 in MCF7 and
242 T47D cells markedly raised the level of FOXO3A (Fig. 3G). To examine whether
243 FRMD8 promotes *ESR1* transcription through FOXO3A, HA-tagged FRMD8 as well
244 as FOXO3A siRNA were co-transfected into MCF7 cells. Although exogenous FRMD8
245 significantly upregulated ERα expression, depletion of endogenous FOXO3A greatly
246 reduced the effect of FRMD8 on ERα (Fig. 3H and 3I). Besides, chromatin
247 immunoprecipitation (ChIP)-qPCR was performed and revealed that depletion of
248 FRMD8 significantly decreased the occupancy of FOXO3A at the *ESR1* promoters (Fig.
249 3J). Altogether, these data indicated that FRMD8 promoted upregulation of *ESR1* is
250 mediated by FOXO3A (Fig. 3K).
251
252 **FRMD8 stabilizes ERα via prevention of its degradation**
253 Although our results suggest that FRMD8 depletion inhibits the mRNA level of *ESR1*,
254 unexpectedly, we also observed that decreased expression of FRMD8 led to a decreased
255 level of exogenous Flag-ERα (Fig. 4A). This result suggested that in addition to
256 inhibiting mRNA expression of ERα, FRMD8 may also regulate ERα protein
257 expression at the post-translational level. To this end, T47D cells were treated with

258 cycloheximide (CHX), a protein synthesis inhibitor. Depletion of FRMD8 greatly
259 increased the ERα turnover rate and the half-life of ERα decreased from 6 h to
260 approximately 2 h (Fig. 4B and 4C). Furthermore, MCF7 and T47D cells were treated
261 with MG132, a proteasome inhibitor, and chloroquine (CQ), a lysosome inhibitor, to
262 determine whether ERα degradation was mediated by the proteasome or the lysosome.
263 The results showed that the reduction of ERα levels by FRMD8 depletion was blocked
264 by treatment with MG132 but not CQ (Fig 4D and 4E). Altogether, these data suggested
265 that FRMD8 stabilizes ERα protein via a proteasome-mediated degradation pathway.
266
267 **FRMD8 inhibits ERα degradation by blocking UBE3A binding with ERα**
268 Given that FERM domain containing proteins play roles via regulating protein-protein
269 interaction, we wonder whether there is an interaction between FRMD8 and ERα. To
270 this end, co-immunoprecipitation (co-IP) assays were performed using Flag-FRMD8 in
271 MCF7 and T47D cells to examine the association of exogenous FRMD8 with
272 endogenous ERα. The results showed that FRMD8 interacts with ERα (Fig. 5A and 5B).
273 Importantly, an interaction between endogenous FRMD8 and endogenous ERα was
274 also observed in MCF7 cells (Fig. 5C). Furthermore, a glutathione S-transferase (GST)
275 pull-down assay using purified recombinant GST-FRMD8 and Flag-tagged ERα
276 proteins was also performed. The results indicated that FRMD8 interacts directly with
277 ERα *in vitro* (Fig. 5D). Taken together, these findings suggest that FRMD8 is a binding
278 partner of ERα in human cells.
279 The aforementioned findings demonstrated that FRMD8 prevents ERα degradation
280 via proteasome pathway. To explore the mechanism by which FRMD8 inhibits ERα
281 degradation, co-IP assay and mass spectrometry (MS) analysis were performed in
282 HEK293A cells transiently expressing Flag-FRMD8 (Table S1). We next searched for
283 the FRMD8-interacting proteins identified by MS matched with the known E3 ubiquitin
284 ligases of ERα. Interestingly, UBE3A, a ubiquitin ligase for ERα(Sun in drugi, 2012),
285 is the only matched protein that interacts with FRMD8 (Fig. 5E). We thus examined the

286 interaction between FRMD8 and UBE3A through co-IP. The results indicated an
287 interaction between FRMD8 and UBE3A (Fig. 5F and 5G). Further, we assumed that
288 FRMD8 may interfere with the interaction between ERα and UBE3A. To test this idea,
289 co-IP assays were performed in HEK293T and T47D cells. In both cell types, the level
290 of ERα ubiquitination and the interaction between ERα and UBE3A were markedly
291 increased by FRMD8 depletion (Fig. 5H and 5I). Intriguingly, FRMD8 depletion led to
292 a marked decrease of ERα expression, while depletion of UBE3A dramatically rescued
293 the effect of FRMD8 depletion (Fig. 5J and 5K). Taken together, these results strongly
294 demonstrated that FRMD8 binds to ERα and UBE3A, and prevents UBE3A interaction
295 with ERα, thereby blocking UBE3A-mediated ERα ubiquitination and degradation (Fig.
296 5L).
297
298 ***FRMD8* promoter is methylated and low FRMD8 level predicts poor prognosis in**
299 **breast cancer patients**
300 Given that Frmd8 prevents mammary tumor growth and inhibits tumor cell
301 proliferation in mice (Fig. 1), we would like to investigate the expression of FRMD8 in
302 breast cancer patients. To this end, whole cell lysates from normal mammary epithelial
303 cells and various subtypes of breast cancer cell lines were subjected to Western blot
304 analysis. Results showed that FRMD8 expression was lower in claudin-low breast
305 cancer cell lines compared with normal mammary epithelial cell line or ERα-positive
306 cell lines (Fig. 6A). Similarly, scRNA-seq results also demonstrated that the level of
307 *Frmd8* in normal Hsd epithelial cells was significantly higher than other tumor cells in
308 the mammary tumors from *PyMT* mice (Fig. 6B).
309 Hypermethylation of tumor suppressor genes is one of the major causes for
310 tumorigenesis. Therefore, we investigated whether the promoter region of FRMD8 is
311 hypermethylated in breast cancer patients. An analysis based on TCGA database
312 showed that the *FRMD8* promoter was highly methylated in primary breast tumors (Fig.
313 6C). Subsequently, breast cancer cells were treated with the DNA methyltransferase

314 inhibitor 5-aza-2-deoxycytidine (5-Aza-dC). The results showed that 5-Aza-dC
315 treatment significantly upregulated both mRNA and protein levels of FRMD8 in
316 claudin-low but not luminal breast cancer cell lines (Fig. 6D, 6E and S4A), which was
317 consistent with the lower expression of FRMD8 in claudin-low breast cancer cell lines
318 (Fig. 6A). These findings demonstrated that *FRMD8* gene promoter is hypermethylated,
319 which could be the reason for the reduced FRMD8 expression in triple-negative breast
320 cancer cells.

321 To further investigate the clinical significance of FRMD8 in breast cancer patients,
322 we performed immunohistochemical staining of FRMD8 in a tissue microarray of
323 breast cancer patients and evaluated the level of FRMD8 (Fig. 6F). The results
324 suggested that patients with lower level of FRMD8 showed poor overall survival
325 ($p$=0.0409) (Fig. 6G). Moreover, we also found that a decreased FRMD8 level was
326 associated with poor recurrence free survival in breast cancer patients according to
327 Kaplan-Meier Plotter analysis (Fig. 6H, 6J, S4B and S4C). Collectively, these data
328 indicated that the promoter of *FRMD8* is hypermethylated, and the low FRMD8 level
329 predicts poor prognosis of breast cancer patients.

330

331 **Discussion**

332 In this study, we found that FRMD8 plays a tumor suppressive role in breast cancer
333 progression. We demonstrated that loss of FRMD8 promotes mammary tumor growth,
334 accelerates the loss of mammary luminal phenotype, and confers tamoxifen resistance
335 via downregulating ERα level. FRMD8 depletion not only suppresses transcription of
336 *ESR1* through decreasing the level of FOXO3A, but also promotes the E3 ligase
337 UBE3A binding with ERα to disrupts ERα protein stability. Moreover, the promoter of
338 *FRMD8* is hypermethylated and a decreased FRMD8 level predicts poor outcomes in
339 breast cancer patients (Fig. 7).

340 As a FERM-domain containing protein, FRMD8 is necessary for releasing of TNF
341 and EGFR ligands(Künzel in drugi, 2018; Oikonomidi in drugi, 2018). FRMD8

342 regulates lung cancer cell growth by regulating tumor microenvironment(Badenes in
343 drugi, 2023). Frmd8-deficient mice are defective in intestinal epithelial barrier repair
344 function and deletion of Frmd8 promotes colorectal tumorigenesis induced by
345 azoxymethane/ dextran sodium sulfate in mice(Badenes in drugi, 2023; Yu in drugi,
346 2023). FRMD8 acts as a scaffold protein, inhibiting CDK4 activation mediated by
347 CDK7 and preventing MDM2-mediated RB degradation(Yu in drugi, 2023). In this
348 study, our results suggested that FRMD8 inhibits mammary tumor progression in
349 *MMTV-PyMT* mice. Besides, FRMD8 also acts as a scaffold molecule, which interacts
350 simultaneously with ERα and UBE3A, and renders UBE3A unable to bind with ERα,
351 thus stabilizing ERα.

352 Specific overexpression of *PyMT* in mammary tissues driven by *MMTV* promoter
353 mimics the signaling of receptor tyrosine kinases activation in human breast
354 cancer(Attalla in drugi, 2021). Gene expression profiling revealed that mammary
355 tumors in *MMTV-PyMT* mice are similar with luminal B subtype of human breast
356 cancer(Pfefferle in drugi, 2013). Early-stage mammary tumors in *MMTV-PyMT* mice
357 express ERα and PR, while they loss ERα and PR as the tumor progresses(Lapidus in
358 drugi, 1998). Our findings suggested that FRMD8 depletion downregulates the level of
359 ERα through a dual mechanism at both the transcriptional and post-translational levels,
360 which accelerates the loss of luminal features in mammary tumor.

361 In this study, we identified that loss of FRMD8 inhibiting *ESR1* expression through
362 downregulating the level of FOXO3A. FOXO3A locates in nucleus and blocks cell
363 cycle progression via activating the cell cycle blocking protein $p27^{KIP1}$ (Seoane in drugi,
364 2004). In addition, FOXO3A contributes to cell death through a Fas ligand-dependent
365 mechanism(Seoane in drugi, 2004). Phosphorylated FOXO3A mediated by AKT binds
366 to 14-3-3 protein and remains in the cytoplasm, resulting in loss of activity(Arden,
367 2004). Thus, FRMD8 may also be involved in the regulation of cell cycle or apoptosis
368 in an ERα-independent manner by regulating FOXO3A. Furthermore, FOXO3A is
369 closely associated with the stemness of breast cancer cells. FOXO3A suppresses breast

370 cancer stem cell properties and tumorigenicity via inhibition of FOXM1/SOX2
371 signaling(Liu in drugi, 2020; Yan in drugi, 2017), suggesting that FRMD8 may have an
372 effect on breast cancer stem cells. However, the mechanisms by which FRMD8
373 promotes FOXO3A expression remain unclear and need to be further investigated.
374 The proportion of luminal subtype is increasing in new cases of breast cancer(Waks
375 in Winer, 2019). Tamoxifen therapy is one of the most important systemic treatment for
376 $ER\alpha^{+}/HER2^{-}$ subtype breast cancer patients(Waks in Winer, 2019). Unfortunately,
377 primary or secondary tamoxifen resistance occurs in about 40% of patients treated with
378 tamoxifen therapy, and tamoxifen resistance often leads to the development of
379 resistance to other selective estrogen receptor modulators(Badia in drugi, 2007; Légaré
380 in Basik, 2016; Rondón-Lagos in drugi, 2016). As a regulator of ERα, FRMD8 may be
381 a therapeutic target for rescue tamoxifen resistance.
382 In summary, we identified FRMD8 as a prognostic marker in breast cancer. FRMD8
383 regulates ERα level through a dual mechanism. Loss of FRMD8 inhibits *ESR1*
384 transcription via downregulating FOXO3A expression. FRMD8 also stabilizes ERα
385 protein by preventing UBE3A from binding to ERα. Deficiency of FRMD8 promotes
386 mammary luminal features loss and confers tamoxifen resistance. Our findings
387 indicated that targeting *FRMD8* promoter methylation may provide a novel therapeutic
388 approach for reversing tamoxifen resistance.
389

## Materials and Methods

### Mice

Both *Frmd8* floxed mice and *MMTV-PyMT* mice were purchased from Shanghai Model Organisms Center Inc (SMOC). *MMTV-Cre*$^{+}$ mice were from the Nanjing Biomedical Research Institute of Nanjing University.

*Frmd8* floxed (*Frmd8*$^{fl/fl}$) mice were crossed with *MMTV-Cre*$^{+}$; *PyMT* transgenic mice to generate *Frmd8* heterozygous (*MMTV-Cre*$^{+}$; *Frmd8*$^{fl/wt}$; *PyMT*) mice. *MMTV-Cre*$^{+}$; *Frmd8*$^{fl/wt}$; *PyMT* mice were further backcrossed with *Frmd8*$^{fl/fl}$ mice to obtain littermate *MMTV-Cre*$^{-}$; *Frmd8*$^{fl/fl}$; *PyMT* and *MMTV-Cre*$^{+}$; *Frmd8*$^{fl/fl}$; *PyMT* mice.

Mice were housed in a pathogen-free animal facility at Laboratory Animal Center of Peking University Health Science Center with a 12 h light/dark cycle, constant temperature and humidity, and fed standard rodent chow and water ad libitum. All animal experiments were approved by the Peking University Biomedical Ethics Committee and the approval number is BCJB0104. Genomic DNA extracted from mouse tail biopsies was subjected to standard genotyping PCR using the primers specified in Table S3. The reaction conditions were: 5 minutes at 94°C; 35 cycles of 30 s at 94°C, 30 s at 56°C and 1 minute at 72°C; followed by 5 minutes at 72°C and hold at 4°C.

### Tamoxifen treatment

7-week-old female mice were given intraperitoneal injections of either corn oil or tamoxifen (50 mg/kg) every two days. Tumor formation was assessed every two days, and the time point at which the tumor first became palpable was recorded as the tumor-free survival time. At the end of the treatment, mice were euthanized and the total number of tumors were counted. Tumors were measured using calipers, and tumor volume was calculated using the formula: $V$ = (length × width × height × 0.5) mm$^3$. Tumors were subsequently fixed in 4% paraformaldehyde (PFA) and housed in individual cassettes for paraffin embedding. 5 μm sections were stained for

418 hematoxylin-eosin (H&E) or immunohistochemistry.

419

420 **Antibodies and reagents**

421 Antibodies against ERα (#8644), Ubiquitin (#3936) and PR (#8757) were purchased
422 from Cell Signaling Technology. Antibodies specific for ERα (#ab32063), CK8
423 (#ab53280), FOXO3A (#ab109629), UBE3A (#ab272168) and HER2 (#ab134182)
424 were from Abcam. Anti-PR (#YM3348) antibody was from Immunoway. Anti-FRMD8
425 (#HPA002861) antibody was from Atlas Antibodies. Anti-Flag (#F3165) antibody was
426 from Sigma-Aldrich. Antibodies against GAPDH (#AC002) was purchased from
427 ABclonal Technology. Anti-Actin (#sc-58673) antibodies was from Santa Cruz
428 Biotechnology. Antibodies specific for β-tubulin (#TA-10) was from Zhong Shan Jin
429 Qiao (ZSGB-Bio).

430 MG132 (#S2619) was purchased from Selleck. Chloroquine (CQ, #C6628),
431 cycloheximide (#C7698) and 5-aza-2-deoxycytidine (5-Aza-dC; #A3656) were
432 purchased from Sigma-Aldrich. Tamoxifen (#HY-13757A) and estradiol (E2, #HY-
433 B0141) were purchased from MedChemExpress.

434

435 **Plasmids**

436 The recombinant vectors encoding human FRMD8 and ERα were constructed by PCR-
437 based amplification, and then subcloned into the p3×Flag-CMV$^{TM}$-10 expression vector.
438 The GST-tagged FRMD8 expression plasmid was generated by inserting PCR-
439 amplified fragments into pGEX-4T-1 vector. All constructs were confirmed by DNA
440 sequencing.

441

442 **Cell culture**

443 Human embryonic kidney cell lines HEK293T and HEK293A and human breast cancer
444 cell lines MCF7, BT-20, MDA-MB-231 and SUM159 were cultured in Dulbecco's
445 Modified Eagle Medium (DMEM). Human breast cancer cell lines T47D and BT-

446 549were cultured in RPMI 1640 medium. All media were supplemented with 10% fetal
447 bovine serum, 100 U/ml penicillin and 0.1 mg/ml streptomycin. Medium for culturing
448 T47D was supplemented with 0.2 U/ml insulin. Human breast cancer cell line MCF10A
449 was cultured in DMEM/F12 medium supplemented with 10% horse serum, 100 U/ml
450 penicillin and 0.1 mg/ml streptomycin, 20 ng/ml epidermal growth factor, 0.5 μg/ml
451 hydrocortisone, 10 μg/ml insulin and 100 ng/ml cholera toxin. All cell lines were
452 maintained in a humidified atmosphere at 37°C with 5% $CO_2$ and passaged using 0.25%
453 trypsin containing 0.02% EDTA for dissociation at 80% confluence.
454
455 **Plasmid and specific siRNA transfection**
456 For transient transfection, cells at 50%-60% confluence were transfected with plasmids
457 via polyethylenimine (PEI; Polyscience, #24765). For RNA interference experiments,
458 cells at 60-70% confluence were transfected with siRNA using Lipo8000 (Beyotime, #
459 C0533). The specific sequences of siRNA are listed in Table S2.
460
461 **Extraction of proteins and immunoblotting**
462 Cells or tissues were lysed using RIPA buffer (1×PBS, pH 7.4, 0.5% sodium
463 deoxycholate, 1% NP-40, and 0.1% SDS) complemented with an EDTA-free cocktail
464 of protease inhibitors (Roche). This was followed by centrifugation at 12,000 rpm for
465 over 15 minutes at a temperature of 4°C to collect the supernatant. Protein
466 concentrations were ascertained using a bicinchoninic acid (BCA) protein assay kit
467 (Applygen, #P1511). Protein samples underwent electrophoresis via SDS-PAGE and
468 were then transferred to a polyvinylidene fluoride (PVDF) membrane employing
469 conventional methods. The membranes were treated with 5% non-fat milk for one hour,
470 then incubated with primary antibodies at 4°C overnight, and subsequently exposed to
471 HRP-conjugated goat anti-mouse or rabbit IgG secondary antibodies for one hour at
472 4°C. The bound antibodies were visualized using the EZ-ECL Chemiluminescence
473 Detection Kit for HRP (Biological Industries, # 20-500-1000) through

474 ChampChemiTM (SageCreation).

475

476 **Chromatin immunoprecipitation**

477 The chromatin immunoprecipitation (ChIP) assay was performed according to the
478 manufacturer's instructions of Sonication ChIP Kit (ABclonal, #RK20258). The
479 purified DNA was analyzed by quantitative reverse transcription PCR (qRT-PCR). All
480 primers are shown in Table S2.

481

482 **Immunoprecipitation**

483 IgG, serving as controls, or indicated antibodies were added to pre-cleared lysates and
484 allowed to incubate overnight at 4°C with sustained rocking. Following this, lysates
485 were subjected to a 4-hour incubation with 35-50 μl of either protein A or protein G
486 Sepharose beads (Santa Cruz Biotechnology) at 4°C. Subsequently, the Sepharose
487 beads were washed thrice with RIPA buffer and heated in SDS-loading buffer at 99°C
488 for 10 minutes. The immunoprecipitation results were assessed via immunoblotting.

489

490 **Mass spectrometry analysis**

491 Flag-FRMD8 and empty vector were transiently transfected in HEK293A cells using
492 PEI, and cell lysates were harvested after 48 h. The cell lysates were pre-cleared and
493 then incubated with pre-washed anti-Flag M2 agarose beads (Yeasen, #20584ES08)
494 overnight at 4°C. Beads were washed three times with PBS. Protein samples were then
495 eluted by boiling with sodium dodecyl sulfate (SDS)-loading buffer at 99°C for 10 min.
496 Ten percent of the samples were saved for immunoblotting. The other 90% of samples
497 were separated by SDS-PAGE, visualized by colloidal coomassie blue staining,
498 destained and subjected to mass spectrometry (MS) analysis.

499 For MS analysis, the protein in the gel was subjected to trypsin digestion. In the LC-
500 MS/MS analysis, the digested products were separated using a 120-minute gradient
501 elution at a flow rate of 0.300 μL/min, utilizing the Thermo Ultimate 3000 nano-UPLC

502 system directly interfaced with the Thermo Fusion LUMOS mass spectrometer. The
503 analytical column used was an Acclaim PepMap RSLC (75 μm ID, 250 mm length,
504 C18). Mobile phase A consisted of 0.1% formic acid, while mobile phase B was 100%
505 acetonitrile with 0.1% formic acid. The Fusion LUMOS mass spectrometer operated in
506 data-dependent acquisition mode, employing Xcalibur 4.1.50 software. It started with
507 a single full-scan mass spectrum in the Orbitrap (375-1500 m/z, 60,000 resolution),
508 followed by data-dependent MS/MS scans. The MS/MS spectra from each LC-MS/MS
509 run were analyzed against the selected database using Proteome Discovery software
510 (version 2.4).
511
512 **Recombinant protein expression and GST pull-down assay**
513 For the expression of Glutathione S-transferase (GST) fusion proteins, GST-tagged
514 recombinant vectors were transfected into *Escherichia coli* Rosetta (DE3) cells. Upon
515 the cell culture attaining an $OD_{600}$ between 0.6 and 0.8, the cells were subjected to
516 overnight incubation with 1 mM isopropyl-β-D-thiogalactopyranoside (IPTG; Sigma,
517 #92320) at 20°C. For the purification of GST fusion proteins, cells were collected and
518 sonicated.
519 For GST-pull down assays, HEK293T cells were transfected and subsequently lysed
520 on ice for over 15 minutes. Purified GST or GST fusion proteins were anchored onto
521 Glutathione Sepharose 4B beads (Pharmacia Biotech). These beads were then further
522 incubated with cellular extract at 4°C for an extended period of over 4 hours, followed
523 by washes with ice-cold PBS for three times. The process concluded with Western blot
524 analysis.
525
526 **RNA extraction and qRT-PCR**
527 Total RNA was isolated using Trizol reagent (Invitrogen) as per the manufacturer's
528 guidelines. 1 μg of the isolated RNA was converted to cDNA using HiScript II Q RT
529 SuperMix for qPCR (+gDNA wiper) (Vazyme). Quantitative real-time PCR, carried out

530 in triplicate, was used to assess relative mRNA levels and was standardized to *GAPDH*
531 expression. The cDNA products were amplified using the LightCycler 96 (Roche)
532 platform, and data were subsequently analyzed through LightCycler 96 (Roche) along
533 with GraphPad Prism 7.0 software. All relevant primers are listed in Table S2.
534
535 **Histology and immunohistochemistry staining**
536 Tissues were preserved in 4% paraformaldehyde, embedded in paraffin, and then sliced
537 into 5 μm sections prior to staining. Following deparaffinization and rehydration, these
538 sections were subject to H&E staining for structural examination.
539 Immunohistochemistry staining was executed using the streptavidin-biotin-peroxidase
540 complex method, with subsequent detection of 3'3'-diaminobenzidine (DAB) as guided
541 by the manufacturer's instructions (Dako, Agilent pathology solutions). Observations
542 and imaging were performed using an Olympus BX51 microscope coupled with an
543 Olympus DP73 CCD photography system.
544
545 **Tumor tissue microarray (TMA) immunohistochemistry analysis**
546 Human breast carcinoma TMA (HBre-Duc140Sur-01) was purchased from Shanghai
547 Biochip. Immunohistochemistry staining for FRMD8 in TMA was performed as
548 described above. The stained microarrays were evaluated by a pathologist blind to
549 cancer outcomes. Based on histological evaluations, staining reactivity was categorized
550 into four levels: absence of reactivity (score=0), weak reactivity (score=1), moderate
551 reactivity (score=2), and intense reactivity (score=3 or 4).
552
553 **Multiple immunohistochemistry staining and analysis**
554 Multicolor immunohistochemistry was conducted using the TissueGnostics Multiple
555 IHC Assay Kit (TissueGnostics, TGFP550) on mammary tumors from mice. Tumors
556 were preserved in 4% paraformaldehyde, embedded in paraffin, and then sliced into 5
557 μm sections prior to staining. The sections were then deparaffinized and hydrated,

558 followed by antigen retrieval in a Tris-EDTA buffer via microwave. Slides underwent
559 treatment with 3% $H_2O_2$ at ambient temperature to eliminate endogenous peroxidase
560 activity. For iterative rounds of cyclic staining, slides were treated with blocking
561 solution, then incubated with the primary antibody either overnight at 4°C or for 2 hours
562 at 37°C, and subsequently with HRP-linked secondary antibody at 37°C for 30 minutes.
563 Signal was enhanced using Tyramide Signal Amplification (TSA) reagents. Antigen
564 retrieval buffer was applied once more, and the aforementioned steps were repeated for
565 additional staining. Lastly, DAPI was used for 10 minutes to stain nuclei. Tissue images
566 were captured using the tissue faxs platform (TissueGnostics).
567 Immunofluorescence image quantification was carried out via StrataQuest v7.0.158
568 software (TissueGnostics). Cells were identified based on DAPI staining, and the
569 expression levels of Frmd8, ERα, PR, and CK8 were calculated by the software,
570 measuring fluorescence intensity and area to enumerate positively-stained cells. The
571 threshold for identifying positive cells was set by inspecting cell recognition on the
572 original image using the View Backward Data function.
573
574 **EdU (5-ethynyl-2'-deoxyuridine) incorporation assay**
575 The EdU incorporation assay was performed according to the manufacturer's
576 instructions of BeyoClick™ EdU Cell Proliferation Kit with Alexa Fluor 488
577 (Beyotime Biotechnology, #C0071) for cell proliferation.
578
579 **Single-cell RNA sequence (scRNA-seq)**
580 Single-cell RNA sequencing libraries were meticulously prepared utilizing the
581 Chromium Single Cell 3' Reagent Kits v3 according to the protocols recommended by
582 10× Genomics. Briefly, an initial quantity of approximately $1\times10^5$ cells, which had
583 been sorted through fluorescence-activated cell sorting (FACS), underwent a triple
584 wash process in DPBS containing 0.04% BSA. These cells were subsequently
585 resuspended to a final concentration of 700 to 1,200 cells/μl, with a minimum viability

586 threshold of 85%. During the library preparation process, cells were encapsulated
587 within droplets to facilitate a precise targeted recovery rate. After the reverse
588 transcription phase, the generated emulsions were disrupted, and the barcoded cDNA
589 was isolated using Dynabeads technology. This was followed by PCR amplification to
590 enrich the cDNA pool. The amplified cDNA served as the template for constructing the
591 3' gene expression libraries. Specifically, for this construction phase, 50 ng of the
592 amplified cDNA was fragmented and subjected to end repair. This material was then
593 subjected to a double-size selection process using SPRIselect beads. The prepared
594 libraries were sequenced on NovaSeq system provided by Illumina, generating 150 bp
595 paired-end reads.
596
597 **Single-cell RNA sequence original data process**
598 Prior to commencing the analysis, cellular data underwent a stringent filtering process.
599 Cells with unique molecular identifier (UMI) counts below 30,000 and those exhibiting
600 gene counts within the range of 200 to 5,000 were excluded. Additionally, cells
601 displaying a mitochondrial content exceeding 20% were also removed from further
602 analysis. Following this preprocessing step, the Seurat package (version 2.3) was
603 employed for both dimensionality reduction and cluster identification. The
604 normalization and scaling of gene expression data were accomplished using the
605 NormalizeData and ScaleData functions, respectively. Subsequently, the
606 FindVariableFeatures function facilitated the selection of the 2,000 genes
607 demonstrating the most significant variation for principal component analysis (PCA).
608 Cluster identification was achieved through the FindClusters function, which
609 partitioned the genes into distinct groups. To mitigate batch effects across samples, the
610 Harmony package was utilized. The refined dataset was then visualized in a two-
611 dimensional space employing Uniform Manifold Approximation and Projection
612 (UMAP) techniques, thereby providing insightful representations of the underlying
613 cellular heterogeneity.

614

615 **Chromosomal copy-number variations estimation**

616 The estimation of chromosomal copy-number variations (CNVs) was conducted
617 utilizing the 'inferCNV' R package. A diverse reference panel comprised of B cells, T
618 cells, NK cells, macrophages and other immune cells facilitated this analysis.
619 Quantification of CNV scores for each subcluster was achieved by aggregating the
620 CNV levels observed across the constituent cells.

621

622 **Quantification and statistical analysis**

623 Statistical comparisons were performed using unpaired two-tailed Student's t tests,
624 Mann Whitney test, one-way ANOVA or two-way ANOVA. Statistical analyses were
625 performed using GraphPad Prism 9.0 software (GraphPad Software, La Jolla, CA,
626 USA). Data are presented as mean ± the standard error of the mean (SEM). Statistical
627 significance was defined as $p<0.05$.

628

## Data Availability

The accession number for the scRNA-seq data reported in this paper is Gene Expression Omnibus (GEO): GSE244582.

## Conflict of Interest Statement

The authors have no potential conflicts of interest.

## Acknowledgments

This study was supported by grants from the Ministry of Science and Technology of China 2022YFA1104003 and 2021YFC2501000; National Natural Science Foundation of China grants 82172972, 82230094, 81972616, 81972609 and 81772840; Peking University Medicine Sailing Program for Young Scholars' Scientific & Technological Innovation BMU2024YFJHPY004; the Fundamental Research Funds for the Central Universities. We would like to thank TissueGnostics Aisa Pacific Limited for their technical support on multiple immunohistochemistry staining.

## Author Contributions

W.W. and M.Y., design, experiment performance, data analyzing, and paper writing; Q.L. and L.Z., bioinformatic analysis; Y.Z., molecular biology-related experiments; Y.S., Z.W. and Y.G., animal experiments; J. Zhang. and Y.T., pathological support; H.Z. and J. Zhan., experimental design, data analysis, and paper writing. All authors have read and approved the manuscript.

## Corresponding Authors

Correspondence to Hongquan Zhang or Jun Zhan.

## References


Arden, K. C. (2004). FoxO: linking new signaling pathways. *Mol Cell*, *14*(4), 416-418. https://doi.org/10.1016/s1097-2765(04)00213-8

Attalla, S., Taifour, T., Bui, T. in Muller, W. (2021). Insights from transgenic mouse models of PyMT-induced breast cancer: recapitulating human breast cancer progression in vivo. *Oncogene*, *40*(3), 475-491. https://doi.org/10.1038/s41388-020-01560-0

Badenes, M., Burbridge, E., Oikonomidi, I., Amin, A., de Carvalho, É., Kosack, L., . . . Adrain, C. (2023). The ADAM17 sheddase complex regulator iTAP/Frmd8 modulates inflammation and tumor growth. *Life Science Alliance*, *6*(4). https://doi.org/10.26508/lsa.202201644

Badia, E., Oliva, J., Balaguer, P. in Cavaillès, V. (2007). Tamoxifen resistance and epigenetic modifications in breast cancer cell lines [Review]. *Current Medicinal Chemistry*, *14*(28), 3035-3043. https://doi.org/10.2174/092986707782794023

Frame, M. C., Patel, H., Serrels, B., Lietha, D. in Eck, M. J. (2010). The FERM domain: organizing the structure and function of FAK. *Nat Rev Mol Cell Biol*, *11*(11), 802-814. https://doi.org/10.1038/nrm2996

Habara, M. in Shimada, M. (2022). Estrogen receptor alpha revised: Expression, structure, function, and stability. *Bioessays*, *44*(12), e2200148. https://doi.org/10.1002/bies.202200148

Jia, X., Li, C., Li, L., Liu, X., Zhou, L., Zhang, W., . . . Shao, Z. M. (2019). Neddylation Inactivation Facilitates FOXO3a Nuclear Export to Suppress Estrogen Receptor Transcription and Improve Fulvestrant Sensitivity. *Clin Cancer Res*, *25*(12), 3658-3672. https://doi.org/10.1158/1078-0432.Ccr-18-2434

Katzenellenbogen, J. A., Mayne, C. G., Katzenellenbogen, B. S., Greene, G. L. in Chandarlapaty, S. (2018). Structural underpinnings of oestrogen receptor mutations in endocrine therapy resistance. *Nature Reviews Cancer*, *18*(6), 377-388. https://doi.org/10.1038/s41568-018-0001-z

Koš, M., Reid, G., Denger, S. in Gannon, F. (2001). Minireview: Genomic Organization of the Human ERα Gene Promoter Region. *Molecular Endocrinology*, *15*(12), 2057-2063. https://doi.org/10.1210/mend.15.12.0731

Künzel, U., Grieve, A. G., Meng, Y., Sieber, B., Cowley, S. A. in Freeman, M. (2018). FRMD8 promotes inflammatory and growth factor signalling by stabilising the iRhom/ADAM17 sheddase complex. *eLife*, *7*, e35012. https://doi.org/10.7554/eLife.35012

Lapidus, R. G., Nass, S. J. in Davidson, N. E. (1998). The loss of estrogen and progesterone receptor gene expression in human breast cancer. *J Mammary Gland Biol Neoplasia*, *3*(1), 85-94. https://doi.org/10.1023/a:1018778403001

Légaré, S. in Basik, M. (2016). Minireview: The link between ERα corepressors and histone deacetylases in tamoxifen resistance in breast cancer [Review]. *Molecular Endocrinology*, *30*(9), 965-976. https://doi.org/10.1210/me.2016-1072

Liu, H., Song, Y., Qiu, H., Liu, Y., Luo, K., Yi, Y., . . . He, Z. (2020). Downregulation

of FOXO3a by DNMT1 promotes breast cancer stem cell properties and tumorigenesis. *Cell Death & Differentiation*, *27*(3), 966-983. https://doi.org/10.1038/s41418-019-0389-3

Moleirinho, S., Tilston-Lunel, A., Angus, L., Gunn-Moore, F. in Reynolds, P. A. (2013). The expanding family of FERM proteins. *Biochem J*, *452*(2), 183-193. https://doi.org/10.1042/BJ20121642

Oikonomidi, I., Burbridge, E., Cavadas, M., Sullivan, G., Collis, B., Naegele, H., . . . Adrain, C. (2018). iTAP, a novel iRhom interactor, controls TNF secretion by policing the stability of iRhom/TACE. *eLife*, *7*, e35032. https://doi.org/10.7554/eLife.35032

Pfefferle, A. D., Herschkowitz, J. I., Usary, J., Harrell, J. C., Spike, B. T., Adams, J. R., . . . Perou, C. M. (2013). Transcriptomic classification of genetically engineered mouse models of breast cancer identifies human subtype counterparts. *Genome Biol*, *14*(11), R125. https://doi.org/10.1186/gb-2013-14-11-r125

Rogatsky, I., Trowbridge, J. M. in Garabedian, M. J. (1999). Potentiation of Human Estrogen Receptor α Transcriptional Activation through Phosphorylation of Serines 104 and 106 by the Cyclin A-CDK2 Complex*. *Journal of Biological Chemistry*, *274*(32), 22296-22302. https://doi.org/https://doi.org/10.1074/jbc.274.32.22296

Rondón-Lagos, M., Villegas, V. E., Rangel, N., Sánchez, M. C. in Zaphiropoulos, P. G. (2016). Tamoxifen resistance: Emerging molecular targets [Review]. *International Journal of Molecular Sciences*, *17*(8), Article 1357. https://doi.org/10.3390/ijms17081357

Seoane, J., Le, H.-V., Shen, L., Anderson, S. A. in Massagué, J. (2004). Integration of Smad and Forkhead Pathways in the Control of Neuroepithelial and Glioblastoma Cell Proliferation. *Cell*, *117*(2), 211-223. https://doi.org/https://doi.org/10.1016/S0092-8674(04)00298-3

Sun, J., Zhou, W., Kaliappan, K., Nawaz, Z. in Slingerland, J. M. (2012). ERα phosphorylation at Y537 by Src triggers E6-AP-ERα binding, ERα ubiquitylation, promoter occupancy, and target gene expression. *Mol Endocrinol*, *26*(9), 1567-1577. https://doi.org/10.1210/me.2012-1140

Sung, H., Ferlay, J., Siegel, R. L., Laversanne, M., Soerjomataram, I., Jemal, A. in Bray, F. (2021). Global Cancer Statistics 2020: GLOBOCAN Estimates of Incidence and Mortality Worldwide for 36 Cancers in 185 Countries. *CA: A Cancer Journal for Clinicians*, *71*(3), 209-249. https://doi.org/https://doi.org/10.3322/caac.21660

Valdes-Mora, F., Salomon, R., Gloss, B. S., Law, A. M. K., Venhuizen, J., Castillo, L., . . . Gallego-Ortega, D. (2021). Single-cell transcriptomics reveals involution mimicry during the specification of the basal breast cancer subtype. *Cell Rep*, *35*(2), 108945. https://doi.org/10.1016/j.celrep.2021.108945

Waks, A. G. in Winer, E. P. (2019). Breast Cancer Treatment: A Review. *JAMA*, *321*(3), 288-300. https://doi.org/10.1001/jama.2018.19323

Williams, C. C., Basu, A., El-Gharbawy, A., Carrier, L. M., Smith, C. L. in Rowan, B. G. (2009). Identification of four novel phosphorylation sites in estrogen receptor α: impact on receptor-dependent gene expression and phosphorylation by protein kinase

CK2. *BMC Biochemistry*, *10*(1), 36. https://doi.org/10.1186/1471-2091-10-36

Yan, H., Li, Q., Wu, J., Hu, W., Jiang, J., Shi, L., . . . Wu, C. (2017). MiR-629 promotes human pancreatic cancer progression by targeting FOXO3. *Cell Death & Disease*, *8*(10), e3154-e3154. https://doi.org/10.1038/cddis.2017.525

Yu, M., Wu, W., Sun, Y., Yan, H., Zhang, L., Wang, Z., . . . Zhang, H. (2023). FRMD8 targets both CDK4 activation and RB degradation to suppress colon cancer growth. *Cell Rep*, *42*(8), 112886. https://doi.org/10.1016/j.celrep.2023.112886

Zhan, J. in Zhang, H. (2018). Kindlins: Roles in development and cancer progression. *Int J Biochem Cell Biol*, *98*, 93-103. https://doi.org/10.1016/j.biocel.2018.03.008

Zhou, W. in Slingerland, J. M. (2014). Links between oestrogen receptor activation and proteolysis: relevance to hormone-regulated cancer therapy. *Nature Reviews Cancer*, *14*(1), 26-38. https://doi.org/10.1038/nrc3622

752 **Figure Legends**

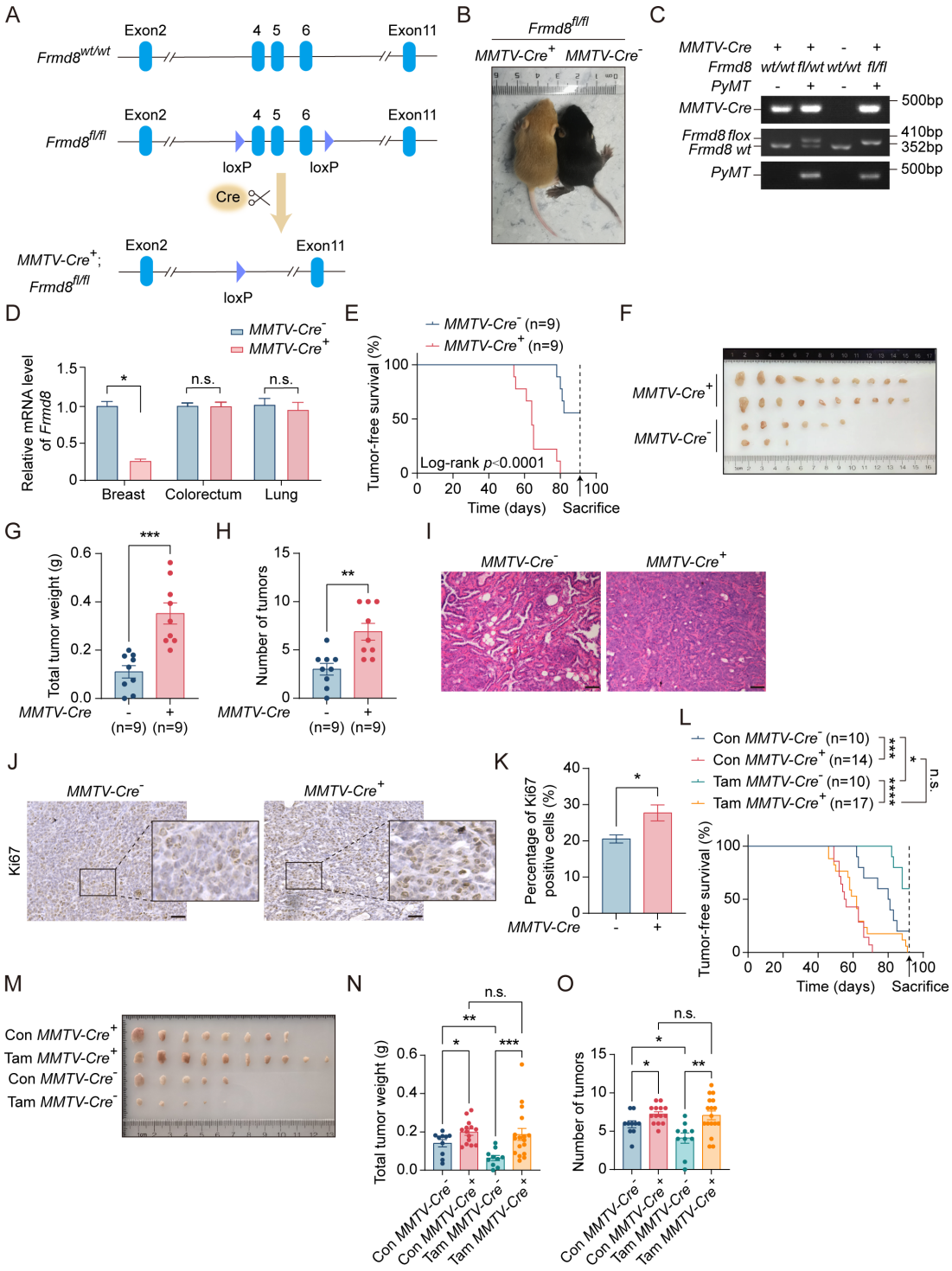


753

754 **Figure 1. Loss of Frmd8 promotes mammary tumor growth and generates**
755 **tamoxifen resistance *in vivo***
756 (A) A diagram of the *Frmd8* targeted alleles. Exons 4, 5 and 6 are flanked by loxp sites.
757 (B) Distinguishing the genotype of littermate mice by mice coat color. Yellow
758 represents *MMTV-Cre*$^{+}$; *Frmd8*$^{fl/fl}$; *PyMT* genotype and black represents *MMTV-Cre*$^{-}$;
759 *Frmd8*$^{fl/fl}$; *PyMT* genotype. (C) Representative PCR genotyping of mouse tail DNA. (D)
760 Relative mRNA level of *Frmd8* in 7-week-old mammary glands from *PyMT* mice was
761 analyzed by qRT-PCR. *Gapdh* was used as an internal reference. *$p$<0.05 by unpaired
762 Student's t-test. (E) Kaplan-Meier plot showing the appearance of palpable tumors in
763 *MMTV-Cre*$^{-}$; *Frmd8*$^{fl/fl}$; *PyMT* (n=9) and *MMTV-Cre*$^{+}$; *Frmd8*$^{fl/fl}$; *PyMT* (n=9) mice
764 (Log-rank test). (F) Representative images of tumors from *MMTV-Cre*$^{-}$; *Frmd8*$^{fl/fl}$;
765 *PyMT* and *MMTV-Cre*$^{+}$; *Frmd8*$^{fl/fl}$; *PyMT* mice. (G-H) Total tumor weight (G) and
766 number of tumors (H) per mice were measured. **$p$<0.01, ***$p$<0.001 by unpaired
767 Student's t-test. (I) Representative H&E staining of tumors from *MMTV-Cre*$^{-}$; *Frmd8*$^{fl/fl}$;
768 *PyMT* and *MMTV-Cre*$^{+}$; *Frmd8*$^{fl/fl}$; *PyMT* mice. Scale bar, 50 μm. (J)
769 Immunohistochemistry (IHC) staining for Ki67 expression in mammary tumors from
770 *PyMT* mice. The black boxes represent the magnified typical staining of the original
771 images. Scale bar, 50 μm. (K) Quantification of Ki67-positive cell percentage in (J).
772 *$p$<0.05 by unpaired Student's t-test. (L) Kaplan-Meier plot showing the appearance of
773 palpable tumors in *MMTV-Cre*$^{-}$; *Frmd8*$^{fl/fl}$; *PyMT* and *MMTV-Cre*$^{+}$; *Frmd8*$^{fl/fl}$; *PyMT*
774 mice, with or without tamoxifen treatment (Log-rank test, *$p$<0.05, ***$p$<0.001,
775 ****$p$<0.0001). (M) Representative images of tumors from *MMTV-Cre*$^{-}$; *Frmd8*$^{fl/fl}$;
776 *PyMT* and *MMTV-Cre*$^{+}$; *Frmd8*$^{fl/fl}$; *PyMT* mice, with or without tamoxifen treatment.
777 (N-O) Total tumor weight (N) and number of tumors (O) per mice from (L) were
778 measured. *$p$<0.05, **$p$<0.01, ***$p$<0.001 by unpaired Student's t-test or Mann
779 Whitney test.
780

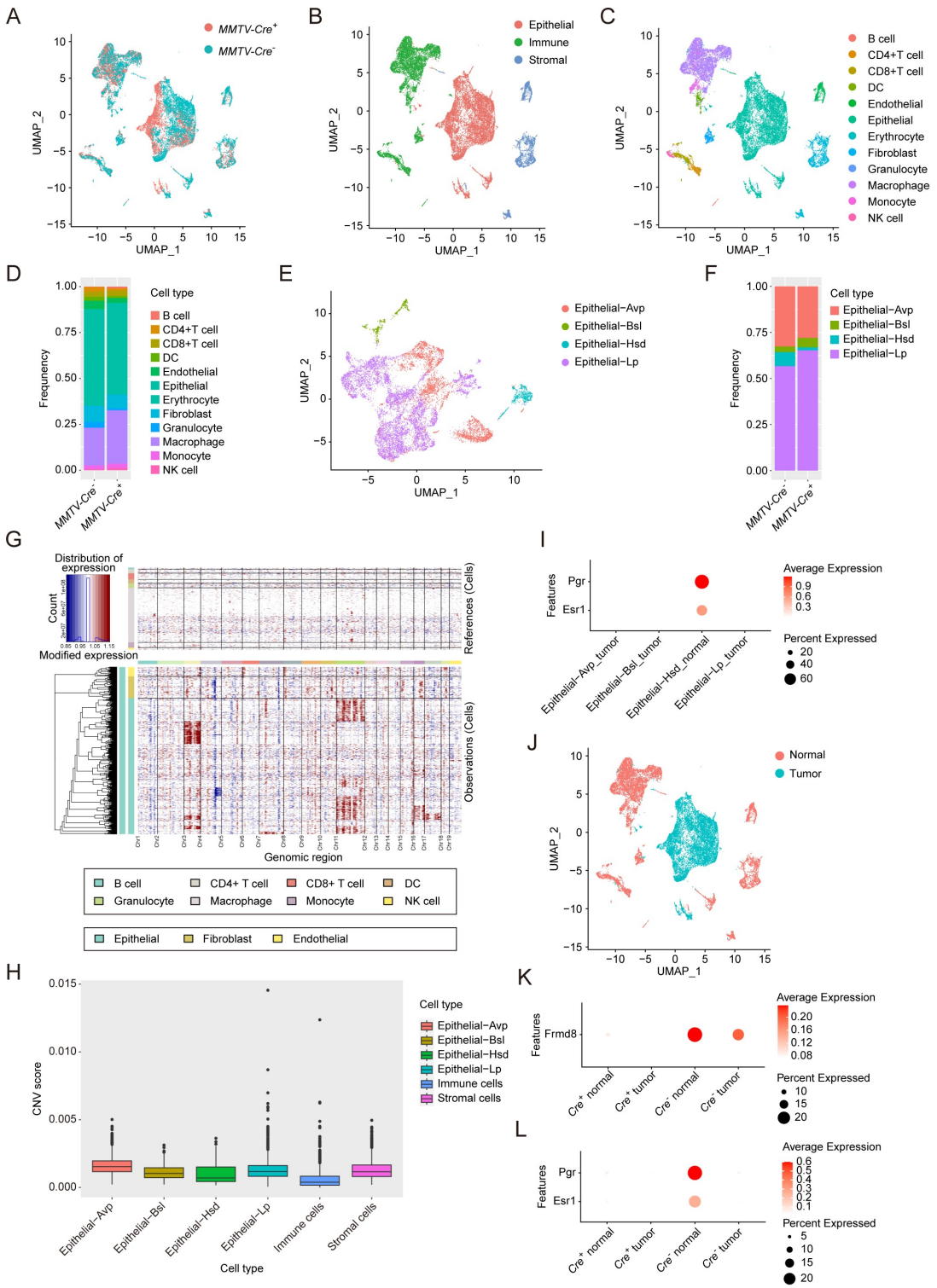


781

782 **Figure 2. Frmd8 knockout decreases the proportion of the hormone-sensing**

783 **differentiated epithelial cells**

784 (A) T-SNE plot showing the distribution of cells from *MMTV-Cre*$^{-}$; *Frmd8*$^{fl/fl}$; *PyMT*

785 and *MMTV-Cre*$^{+}$; *Frmd8*$^{fl/fl}$; *PyMT* mice. (B) T-SNE plot showing the distribution of

786 epithelial, immune and stromal cells. (C-D) T-SNE plot showing the distribution of
787 main cell linages (C) and their relative percentage (D). (E-F) T-SNE plot showing the
788 distribution of epithelial cell linages (E) and their relative percentage (F). (G) Heatmap
789 showing distinct features of each cell lineages. Rows, genes. Columns, cells. The color
790 key from blue to red indicates low to high gene expression. (H) Boxplot showing CNV
791 score of main cell linages. (I) Dot plot showing the expression of *Esr1* and *Pgr* in
792 epithelial cell linages. (J) T-SNE plot showing the distribution of normal cells and tumor
793 cells. (K) Dot plot showing the expression of *Frmd8* in normal and tumor cells from
794 *MMTV-Cre*$^{-}$; *Frmd8*$^{fl/fl}$; *PyMT* and *MMTV-Cre*$^{+}$; *Frmd8*$^{fl/fl}$; *PyMT* mice. (L) Dot plot
795 showing the expression of *Esr1* and *Pgr* in normal and tumor cells from *MMTV-Cre*$^{-}$;
796 *Frmd8*$^{fl/fl}$; *PyMT* and *MMTV-Cre*$^{+}$; *Frmd8*$^{fl/fl}$; *PyMT* mice.
797

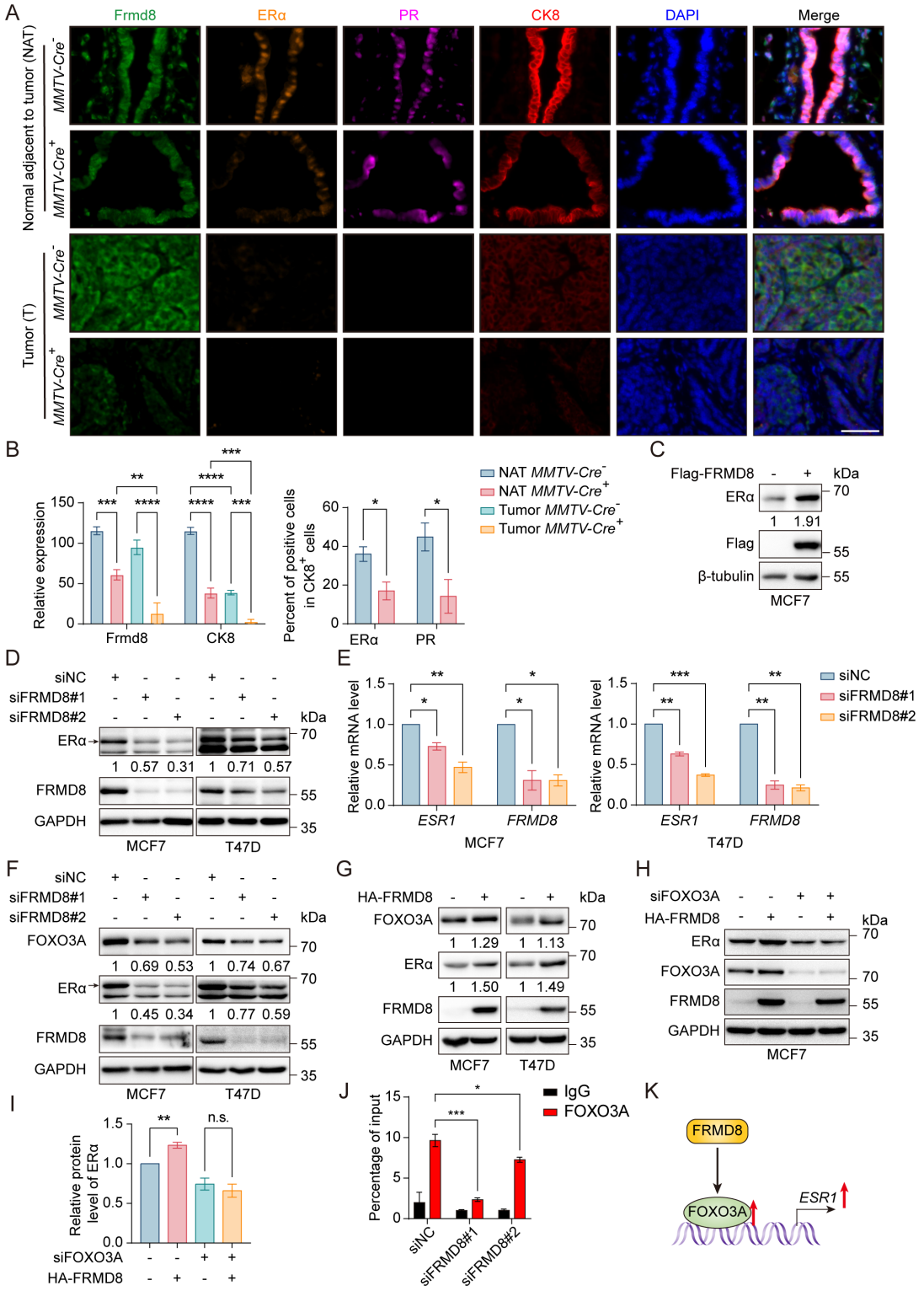


**Figure 3. FRMD8 promotion of *ESR1* expression is mediated by FOXO3A**

(A) Representative multiplex immunofluorescence images of tumor tissues and tissues adjacent to tumor from *MMTV-Cre*$^{-}$; *Frmd8*$^{fl/fl}$; *PyMT* and *MMTV-Cre*$^{+}$; *Frmd8*$^{fl/fl}$; *PyMT* mice. Scale bar, 50 μm. (B) Qualification of Frmd8 and CK8 expression (left

803 panel) and ERα and PR-positive cell percentage in $CK8^+$ cells (right panel) in (A).
804 *$p$<0.05, **$p$<0.01, ***$p$<0.001, ****$p$<0.0001 by one-way ANOVA (left panel) or
805 unpaired Student's t-test (right panel). (C) Lysates from MCF7 cells transiently
806 transfected with Flag or Flag-FRMD8 were immunoblotted. (D) Lysates from MCF7
807 and T47D cells transiently transfected with control or FRMD8 siRNA were
808 immunoblotted. In this and subsequent figures, specific bands are marked with an arrow.
809 (E) Relative mRNA levels of *ESR1* and *FRMD8* from MCF7 and T47D cells transiently
810 transfected with control or FRMD8 siRNA were analyzed by qRT-PCR. *GAPDH* was
811 used as an internal reference. *$p$<0.05, **$p$<0.01, ***$p$<0.001 by one-way ANOVA.
812 (F) Lysates from MCF7 and T47D cells transiently transfected with control or FRMD8
813 siRNA were immunoblotted. (G) Lysates from MCF7 and T47D cells transiently
814 transfected with HA or HA-FRMD8 were immunoblotted. (H-I) Lysates of MCF7 cells
815 co-transfected with HA-FRMD8 and FOXO3A siRNA as indicated were
816 immunoblotted (H). ERα protein levels were quantified by normalizing to the intensity
817 of the GAPDH band (I). **$p$<0.01 by unpaired Student's t-test. (J) Lysates of T47D
818 cells transfected with control or FRMD8 siRNA were subjected to anti-FOXO3A ChIP-
819 qPCR. *$p$<0.05, ***$p$<0.001 by one-way ANOVA. (K)Working model for FRMD8
820 promotes *ESR1* transcription via upregulating FOXO3A expression.
821

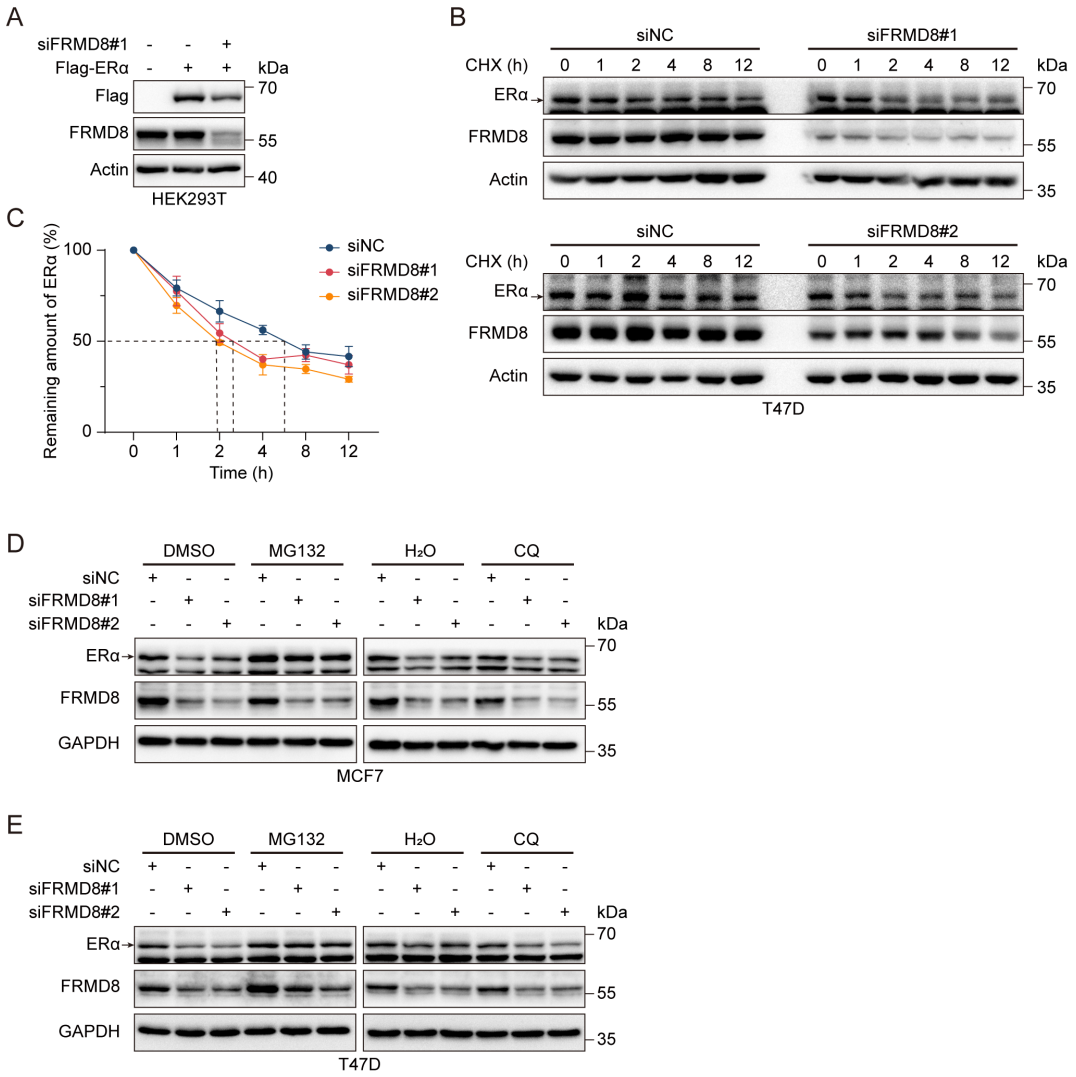


**Figure 4. FRMD8 stabilizes ERα via prevention of its degradation**

(A) Lysates of HEK293T cells co-transfected with Flag-ERα and FRMD8 siRNA as indicated were immunoblotted. (B-C) Lysates from T47D cells transiently transfected with control or FRMD8 siRNA were subjected to immunoblotting. Cells were treated with 100 μg/ml CHX for the indicated times (B). ERα protein levels were quantified by normalizing to the intensity of the Actin band (C). (D-E) Immunoblot analysis of ERα in MCF7 (D) and T47D (E) cells transiently transfected with control or FRMD8 siRNA. The cells were treated with MG132 (25 μM) or chloroquine (50 μM) for 6 h.

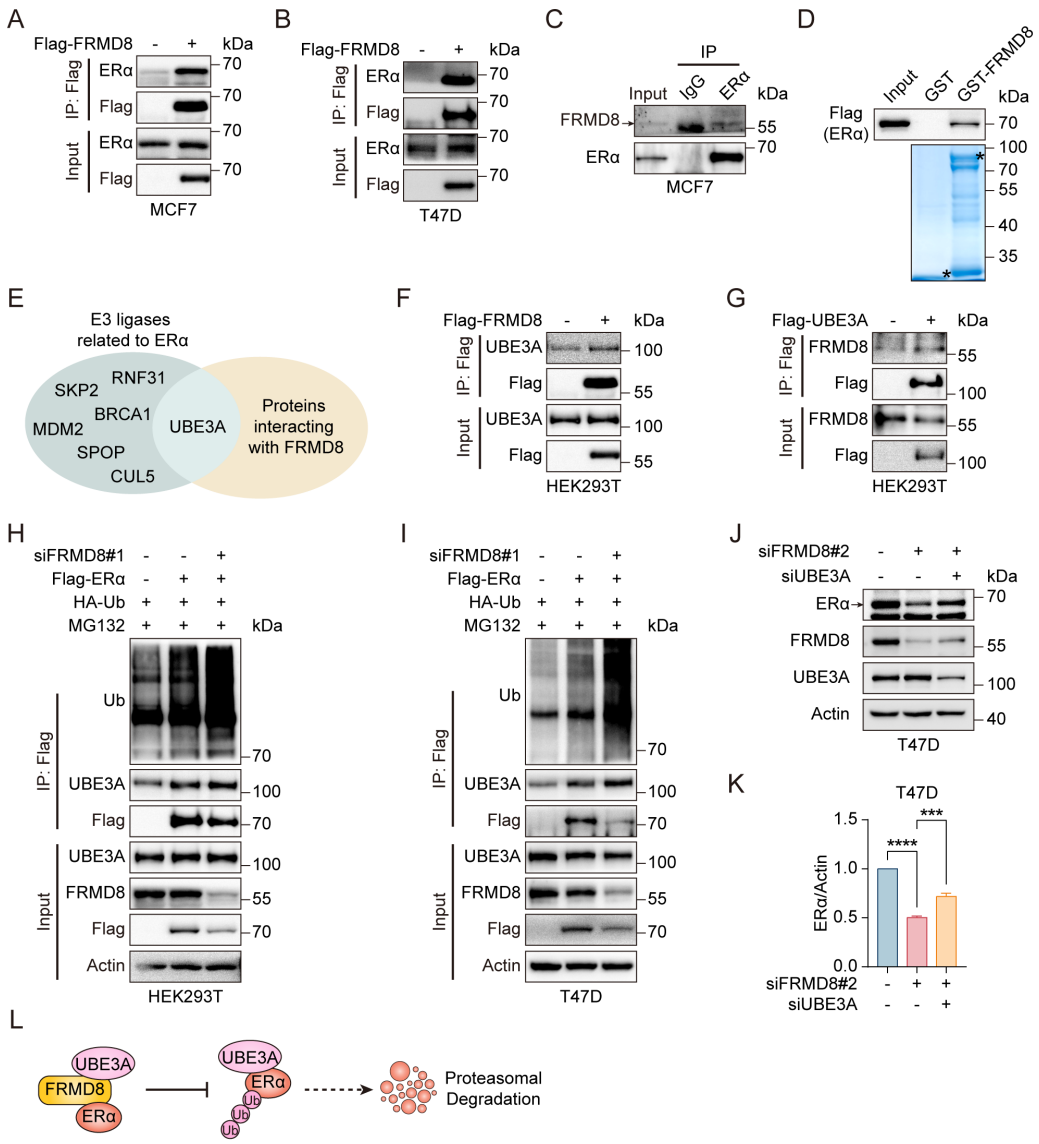


**Figure 5. FRMD8 inhibits ERα degradation by blocking UBE3A binding with ERα**

(A-B) Lysates of MCF7 (A) and T47D (B) cells transfected with Flag or Flag-FRMD8 were anti-Flag immunoprecipitated and immunoblotted for ERα and Flag. (C) Lysates from MCF7 cells were immunoprecipitated with IgG or anti-ERα, then immunoblotted for FRMD8 and ERα. (D) HEK293T cells were transiently transfected with Flag-ERα. ERα proteins in HEK293T whole cell lysates (WCL) pulled down by GST or GST-FRMD8 recombinant proteins were subjected to Western blot. Asterisks indicate proteins at the expected molecular weight. (E) Venn diagram showing overlap of E3 ligases related to ERα and proteins interacting with FRMD8. (F) Lysates of HEK293T cells transfected with Flag or Flag-FRMD8 were anti-Flag immunoprecipitated and

843 immunoblotted. (G) Lysates of HEK293T cells transfected with Flag or Flag-UBE3A
844 were anti-Flag immunoprecipitated and immunoblotted. (H-I) HEK293T (H) and T47D
845 (I) cells were co-transfected with Flag-ERα, HA-Ub and FRMD8 siRNA as indicated.
846 Cells were treated with MG132 (25 μM) for 6 h. WCL were immunoprecipitated with
847 anti-Flag and then immunoblotted for ubiquitinated ERα. (J-K) Lysates of T47D cells
848 co-transfected with FRMD8 and UBE3A siRNA as indicated were immunoblotted (J).
849 ERα protein levels were quantified by normalizing to the intensity of the Actin band
850 (K). ***$p<0.001$, ****$p<0.0001$ by one-way ANOVA. (L) Working model for FRMD8
851 disrupts the interaction between ERα and UBE3A, and protects ERα from UBE3A-
852 mediated degradation.
853

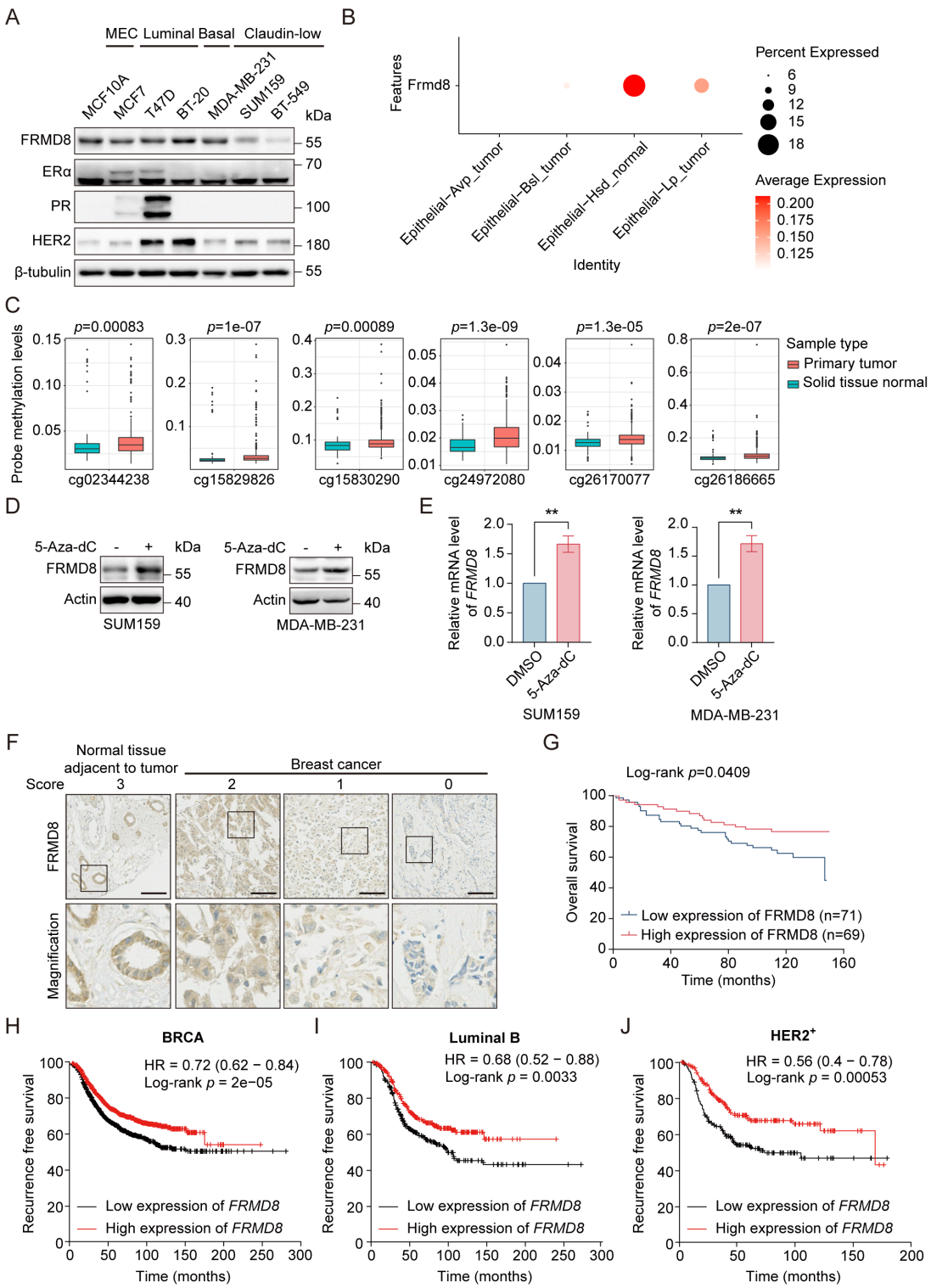


854

855 **Figure 6. *FRMD8* promoter is methylated and low FRMD8 level predicts poor**

856 **prognosis in breast cancer patients**

857 (A) Lysates from human mammary epithelial cell (MEC) and breast cancer cells were

858 subjected to immunoblotting. (B) Dot plot showing the expression of *Frmd8* in

859 epithelial cell linages from *PyMT* mice. (C) Methylation of *FRMD8* promoter region in
860 breast cancer according to the University of California Santa Cruz (UCSC) database
861 (http://xena.ucsc.edu/). (D) SUM159 and MDA-MB-231 cells were treated with 5-Aza-
862 dC (10 μM) for 48 h. Protein expression of FRMD8 was examined by Western blot. (E)
863 SUM159 and MDA-MB-231 cells were treated with 5-Aza-dC (10 μM) for 48 h.
864 *FRMD8* mRNA levels was examined by quantitative reverse transcription PCR (qRT-
865 PCR) *GAPDH* was used as an internal reference. $^{**}p<0.01$ by unpaired Student's t-test.
866 (F) IHC analysis of FRMD8 expression in human breast carcinoma TMA was
867 performed. Representative examples (scale bar, 100 μm) of normal tissue adjacent to
868 tumor and breast cancer with different levels of FRMD8 expression are shown, with
869 the magnification of selected areas inserted. (G) Kaplan-Meier analysis for the overall
870 survival of breast cancer patients according to FRMD8 expression (Log-rank test). (H-
871 J) Recurrence free survival of breast cancer patients according to *FRMD8* expression
872 were analyzed according to Kaplan-Meier plotter (http://kmplot.com/analysis/).
873

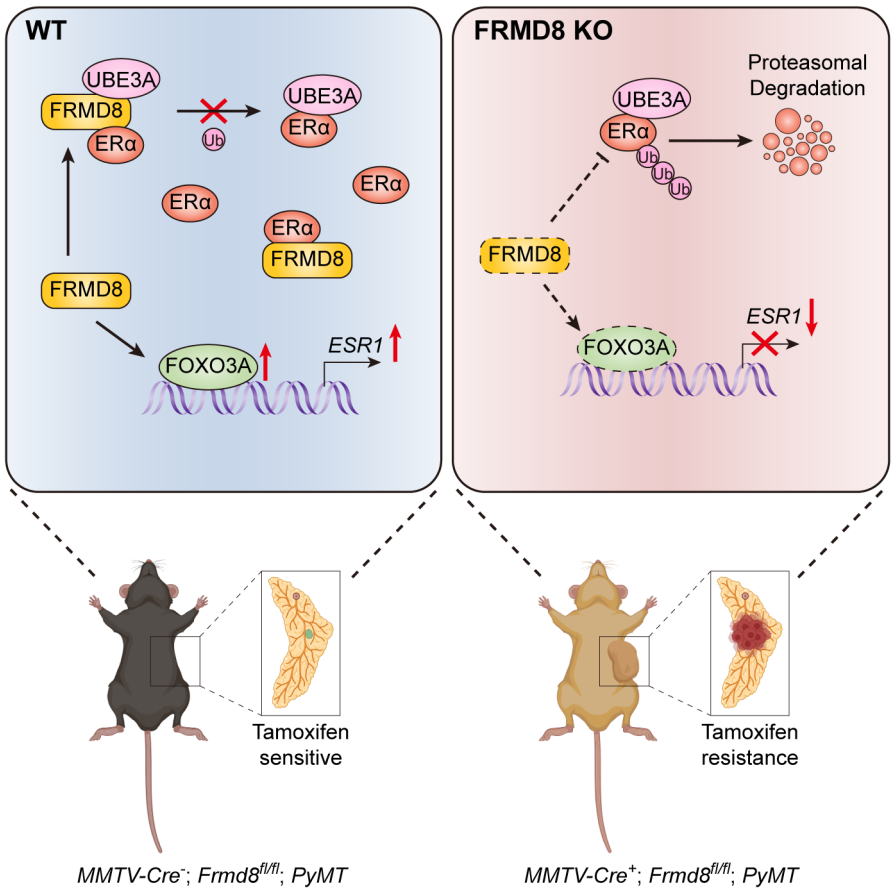


874

875 **Figure 7. A working model shows that loss of FRMD8 promotes mammary tumor**

876 **progression and confers tamoxifen resistance by downregulating ERα expression**

877 **at both transcriptional and post-translational levels.**